

【Review Paper】

Interfacial dynamics in complex fluids

James J. FENG* and Ching-Yao CHEN**

* Department of Chemical and Biological Engineering and Department of Mathematics
University of British Columbia, Vancouver, BC V6T 1Z2, Canada
E-mail: james.feng@ubc.ca

** Department of Mechanical Engineering, National Chiao Tung University
Hsin Chu, Taiwan, ROC

Received 24 February 2016

Abstract

Complex fluids are characterized by microstructures whose configuration can be driven out of equilibrium by macroscopic flow, and consequently contribute an additional stress that modifies the flow in return. When immiscible complex fluids coexist in a flow system, the fluid-fluid interface introduces an additional length scale into the fluid dynamics, typically intermediate between the microstructures of the bulk fluids and the macroscopic flow. Thus, multicomponent complex fluids often exhibit intriguing features in the interfacial flow, and offer an opportunity to study hydrodynamic coupling across length scales. In this review, we illustrate the novel interfacial dynamics in complex fluids using three examples that involve three types of complex fluids: polymer solutions, liquid crystals and ferrofluids. The focus will be on the dynamics of drops, which coalesce, break up, and self-assemble into regular patterns in these examples. In each case, we present experimental observations of novel interfacial phenomena. Then we explore the underlying fluid-dynamic mechanisms using theoretical models and numerical simulations. Comparing the experimental and computational results, we highlight the roles of the interface in relating complex rheology on the molecular scale to hydrodynamics on the macroscopic scale. Finally we point out outstanding questions and suggest future investigations.

Key words : Viscoelasticity, Partial coalescence, Distortional elasticity, Self-assembly, Pattern formation, Ferrofluids, Cahn-Hilliard equation, Maxwell stress tensor

1. Introduction

The subject of this review is at the intersection of two lines of fluid mechanical research: complex fluids and multiphase fluids. Complex fluids have microstructures whose conformation can be perturbed by macroscopic flow. Once out of equilibrium, these microstructures give rise to a non-Newtonian stress tensor that modifies the flow field in return (Larson, 1999). This behavior contrasts that of “simple fluids” such as water. Although water can be said to possess a microstructure in its molecular structure, the vibration of the chemical bonds is so fast that this has no bearing on the macroscopic flow of water. An important class of complex fluids are polymer solutions and melts that exhibit viscoelasticity, with a fading memory determined by the relaxation time of the polymer chains or their entanglements (Bird *et al.*, 1987*a,b*; Doi & Edwards, 1986). Liquid crystals are another class of complex fluids (de Gennes & Prost, 1993). Here the microstructure is the rod-like or disc-like molecules that tend to align with each other. As this alignment extends in space, a long-range orientational correlation arises, giving rise to distortional elasticity and endowing liquid crystals a fluid-solid duality. Yet another kind of complex fluids is ferrofluids, colloids with nano-size magnetic particles suspended in an oil- or water-based liquid matrix. The particles are sufficiently fine that the ferrofluid behaves as a homogeneous continuum, yet they allow an external magnetic field to apply body forces to the fluid and drive novel phenomena (Odenbach, 2002; Rosensweig, 1997).

In general, multiphase fluid dynamics deals with mixtures of gases, liquids and solids. Of special relevance here are *multi-component* liquid-liquid mixtures. An oil-water emulsion, for example, exhibit complex rheology because the interfaces move, deform, break up and coalesce during deformation, and their location and conformation are not known

a priori (Larson, 1999). In this review, we will consider multicomponent mixtures of complex fluids, with evolving interfaces that separate complex fluids. This brings together three length scales, with the *microscopic* dynamics within the bulk fluid producing non-Newtonian stresses, and the interfaces deforming and restructuring on the *mesoscopic* scale in reaction to such stresses, and ultimately modifying the *macroscopic* flow. Of course, the flow of information goes in the reverse direction as well, with macroscopic flow affecting the interfaces and in turn the molecular conformation within each component.

We are attracted to this kind of fluid systems for two main reasons. The first is a fundamental interest in the fluid dynamics of such materials. They provide a unique opportunity to probe novel flow phenomena that arise from the multi-scale coupling. Examples of these will be described in the next section. Often surprising or counterintuitive, these observations enrich our understanding of fluid dynamics and broaden the research forefront of the field. The second attraction comes from the practical importance of mixtures of complex fluids in engineering applications. By blending polymers of complementary properties, for example, one can produce high-performance, light-weight composite materials for structural applications in automotive and aerospace sectors (Thomas *et al.*, 2015). Dispersing droplets of liquid crystalline polymers in a matrix of isotropic flexible-chain polymers produces polymer-dispersed liquid crystals that is a promising route to flexible optical displays and “smart glass” (Bloisi & Vicari, 2012). Finally, ferrofluids can be used as liquid seals and mechanical actuators and dampers, among other applications (Odenbach, 2002).

In the rest of this article, we will use several concrete phenomena to illustrate the unusual interfacial dynamics in complex fluids. These include suppression of partial coalescence in polymer solutions, interaction and self-assembly of droplets in a liquid crystal medium and breakup and self-assembly of ferrofluid drops. Needless to say, the choice of problems largely reflects the authors’ own interests and experiences. If not the “best” examples for the current purpose, they are illustrative and have the advantage of being familiar to the authors. In the same spirit, the review will not attempt to be complete or exhaustive. For each process, we will mention certain earlier work that is most relevant to the narrative, but have to omit many other important contributions. After describing experimental observations in each case, we will also present theoretical analysis and numerical simulations that explore the underlying hydrodynamic mechanisms, which invariably boil down to the coupling across the microscopic, mesoscopic and macroscopic scales. Finally, we will highlight existing puzzles in this area and suggest future research directions.

2. Suppression of partial coalescence by viscoelasticity

Consider the interface between a polymer solution and a Newtonian viscous fluid. On the polymer side, deformation will induce viscoelastic stresses that will make the interfacial behavior markedly different from that of Newtonian fluids. A striking example of this effect is the well-known beads-on-string phenomenon (Fontelos & Li, 2004; Oliveira & McKinley, 2005). On a filament of a viscoelastic polymer solution, the appearance of capillary waves is followed by thinning of the thread but not rapid breakup by Rayleigh instability. Instead, smaller beads form between the larger ones as the thread continues to thin. In the end, several generations of beads coexist and persist for a long time before breakup (Oliveira & McKinley, 2005). The longevity of the thread is due to the long polymer chains in the solution. The thinning of the thread stretches and aligns the chains, which drastically increases the filament’s elongational viscosity, namely its resistance to further thinning and breakup. The phenomenon to be discussed below is another manifestation of the power of viscoelastic stress in modifying interfacial dynamics.

2.1. Experimental observations

Consider a stationary oil layer sitting on top of a water layer that is denser than the oil. Now gently deposit a water drop on the oil-water interface. The drop squeezes the oil film below and eventually coalesces with the water below. Under favorable conditions, “partial coalescence” obtains in which a smaller daughter drop is left on the interface (Fig. 1). It then repeats the film drainage process until coalescence, which may leave a still smaller daughter drop on the interface. Such a cascade of partial coalescence has been documented with high-speed video both for liquid-liquid systems (Charles & Mason, 1960; Chen *et al.*, 2006*a,b*; Gilet *et al.*, 2007; Mohamed-Kassim & Longmire, 2004; Nikolov & Wasan, 1995) and for air-liquid systems (Blanchette & Bigioni, 2006; Honey & Kavehpour, 2006; Thoroddsen & Takehara, 2000). Furthermore, the partial coalescence occurs only for an intermediate range of drop sizes. Drops too large or too small coalesce with the underlying liquid in one shot.

What causes a daughter drop to be left behind, and why does this happen for intermediate drop sizes? The answer can be sought from the interfacial dynamics shown in Fig. 1. The onset of coalescence sends a capillary wave up the

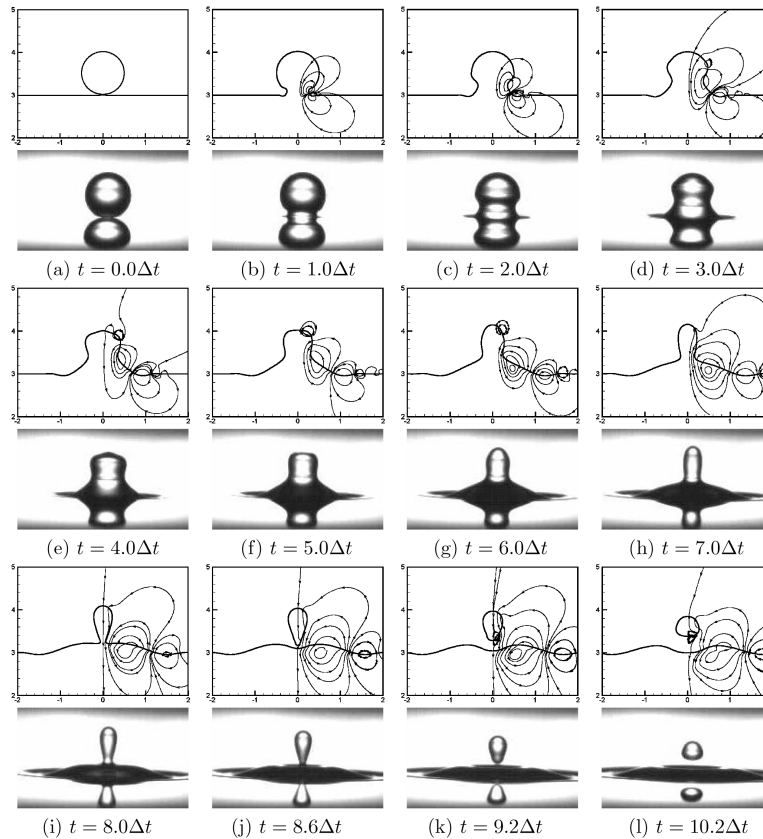


Fig. 1 Partial coalescence in a Newtonian-Newtonian system. The upper fluid is decane, and the lower fluid and the drop are water. The snapshots are experimental images separated by a constant time interval $\Delta t = 542 \mu\text{s}$. For a frame-by-frame comparison between observation and simulation of one cycle of partial coalescence, we select the numerical images that best approximate the experimental ones, and indicated the numerical time below each pair of images. Streamlines in the computational plot indicate the local flow field. From Yue *et al.* (2006a) with permission, ©2006 American Institute of Physics.

drop, turning it into an elongated liquid column. This is a process of surface energy being converted to kinetic and then gravitational potential energy. The column becomes unstable to Rayleigh instability and a neck starts to form near its base. Hence two time scales come into competition. If it takes longer to drain the drop through the neck than for the neck to pinch off, then pinch-off occurs and leaves a daughter drop behind. Conversely, if the drop drains into the lower layer before the neck pinches off, complete coalescence results. For drops that are too large, gravity dominates and the drop practically collapses into the bottom layer in one shot. For drops that are too small, viscosity dominates and slows down the thinning of the neck so complete merging takes place.

What if one of the liquid phases is viscoelastic? Chen *et al.* (2006b) explored the same process when the drop or the underlying liquid is a polymer solution. The non-Newtonian rheology, as it turns out, tends to suppress partial coalescence; under conditions that would have led to partial coalescence for Newtonian fluids, now the coalescence is completed at once (Fig. 2). The suppression may occur if the polymer solution constitutes either the drop or the surrounding fluid, and the effect is stronger in the former case.

This effect can be understood by contrasting the Newtonian and viscoelastic scenarios depicted in Figs. 1 and 2. Up to the onset of the neck formation, the Newtonian and viscoelastic behaviors are qualitatively the same. For the viscoelastic column of Fig. 2, the viscoelastic effect evident in the beads-on-a-string formation plays a similar stabilizing role against Rayleigh instability. The neck turns into a thin filament (Frame 5 of Fig. 2), but it persists without breaking up. In time the drop fluid drains down the filament and the shrinking drop falls and merges into the underlying polymer solution. Thus, partial coalescence is suppressed. To explain the inverted case of a Newtonian drop in a polymeric upper liquid, Chen *et al.* (2006b) observed the breakup of a Newtonian filament in a polymer solution, and found that it is subject to the same type of stabilization with the formation of beads on the thinning thread.

The suppression of partial coalescence by viscoelasticity clearly demonstrates how bulk rheology qualitatively modifies the behavior of the interface. Here the rheology is manifested by “strain hardening”, namely a steep increase in

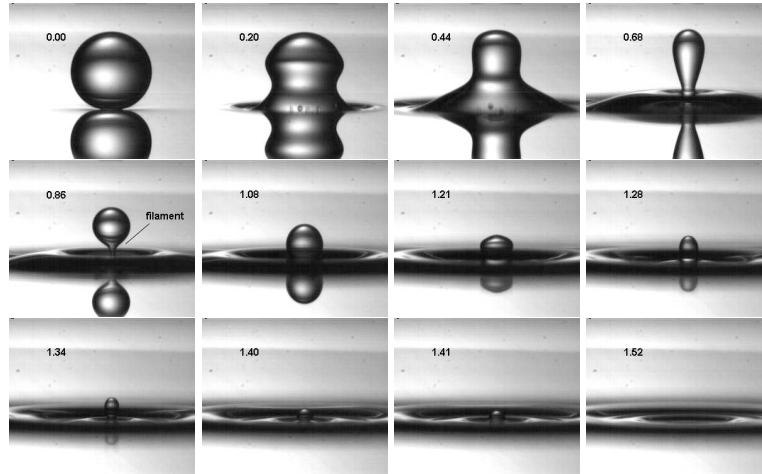


Fig. 2 Suppression of partial coalescence by viscoelasticity. The drop fluid is a 0.18% solution of poly(ethylene oxide) in water, and the surrounding liquid is decane. The initial drop diameter $D = 1.8$ mm, and the numbers in the frames indicate the advance in time scaled by the capillary time $t_c = (\rho D^3 / \sigma)^{1/2}$, ρ and σ being the fluid density and interfacial tension. From Chen *et al.* (2006b) with permission, ©2006 American Institute of Physics.

elongational viscosity during stretching. Its molecular origin is the stretching and alignment of polymer chains by the elongational flow. While the qualitative explanation above sounds reasonable, a quantitative study of the fluid mechanical process is necessary.

2.2. Numerical simulations

To simulate the partial coalescence and its suppression, and interfacial flows of complex fluids in general, we need to deal with two complications beyond that of solving the Navier-Stokes equations. One is the non-Newtonian stress tensor and the other is the interfacial motion and deformation. For viscoelastic liquids, the stress tensor $\boldsymbol{\tau}$ depends not only on the deformation at the current moment, but also the history of deformation (Bird *et al.*, 1987a,b; Larson, 1999). As an example, we write the constitutive equation for the Giesekus model, where the total stress tensor $\boldsymbol{\tau}$ is the sum of a Newtonian contribution and a polymer stress $\boldsymbol{\tau}_p$, the latter determined by:

$$\boldsymbol{\tau}_p + \lambda_H \left[\frac{\partial \boldsymbol{\tau}_p}{\partial t} + \mathbf{v} \cdot \nabla \boldsymbol{\tau}_p - (\nabla \mathbf{v})^T \cdot \boldsymbol{\tau}_p - \boldsymbol{\tau}_p \cdot \nabla \mathbf{v} \right] + \alpha \frac{\lambda_H}{\mu_p} \boldsymbol{\tau}_p \cdot \boldsymbol{\tau}_p = \mu_p [\nabla \mathbf{v} + (\nabla \mathbf{v})^T], \quad (1)$$

where λ_H and α are the relaxation time and mobility parameter, and μ_p is the polymer viscosity.

As the motion of the interfaces has to be solved for along with the fluid flow, we use an interface capturing method known as the diffuse-interface model (Feng *et al.*, 2005; Yue *et al.*, 2004). A phase-field variable is introduced to demarcate the fluid components, and the interfacial motion is extracted from the evolution of the phase field governed by the Cahn-Hilliard equation. The interfacial tension is treated as a body force that acts within a thin interfacial layer. The theoretical background of the model and its computational implementation have been discussed in the literature (Feng *et al.*, 2005; Yue *et al.*, 2006b; Zhou *et al.*, 2010). For the problems at hand, this formalism enjoys the advantage that the moving interface and viscoelastic rheology can be handled in a unified framework based on the free energy.

To validate the model and the numerical scheme, we reproduce the partial coalescence experiment for Newtonian liquids, with a water drop above a decane-water interface (Yue *et al.*, 2006a) (Fig. 1). Following the initial rupture at $t = 0$, the numerical simulation accurately reproduces the progress of the coalescence, from the propagation of the capillary wave up the drop (a–e) to the formation of a liquid column (e–g), and finally to the formation of a neck (g–i). The next 2 frames, however, cover the pinchoff of the neck that generates the daughter drop. This is when the numerical simulation fails to track the progression in the correct time; the pinchoff occurs some 40% faster numerically than in reality. After the daughter drop is formed (k), the simulation again captures the real event precisely. The discrepancy for frames (j) and (k) highlights a fundamental limitation to the diffuse-interface method. Limited by computational capacity, the interfacial thickness used in the simulation is typically much greater than the real value, which is on the nanometer scale for small-molecule liquids. This thickness is immaterial as long as the physical length scale of interest is much larger. Near pinch-off, however, when two interfaces approach each other, interfacial diffusion becomes appreciable. This makes the pinch-off proceed faster in the simulation. Note, however, that this limitation is by no means specific to

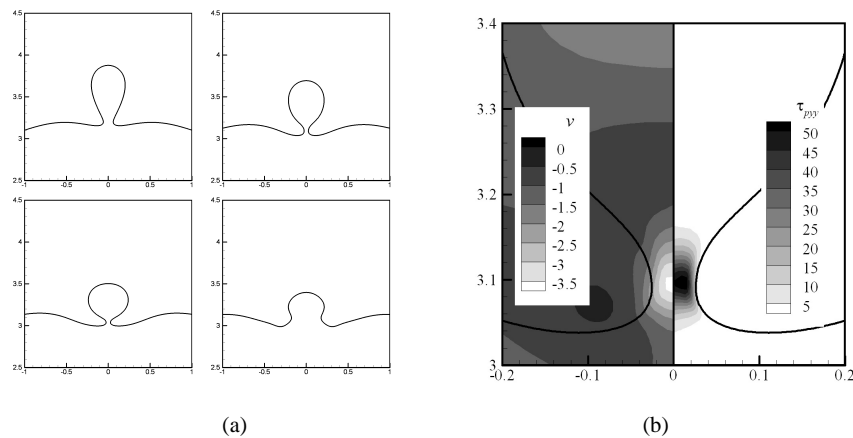


Fig. 3 Suppression of partial coalescence by viscoelasticity. The drop and lower fluid is a viscoelastic Giesekus fluid, while the upper layer is a Newtonian fluid. (a) From left to right and then top to bottom, the snapshots are at dimensionless times $t = 0.740, 0.837, 0.934$ and 1.04 , scaled by the capillary time t_c . (b) Flow and stress fields near the neck of the viscoelastic drop at $t = 0.837$. The left half shows contours of the vertical velocity scaled by D/t_c . The right half shows contours of the polymer stress component τ_{pyy} scaled by σ/D . From Yue *et al.* (2006a) with permission, ©2006 American Institute of Physics.

the diffuse-interface method. All numerical methods struggle to cover a large separation of length scales. That partial coalescence occurs only for a range of drop sizes, being suppressed by gravity and viscosity on either end of the range, has also been reproduced numerically (Yue *et al.*, 2006a).

To explore how viscoelasticity suppresses partial coalescence, we use the Giesekus constitutive equation (Eq. 1), with model parameters fitted roughly to the rheology of the polymer solutions. Figure 3(a) shows the evolution of the interfaces for a polymer drop surrounded by a Newtonian oil. The neck forms but the thin thread persists without breaking, as seen experimentally in Fig. 2. The evolution of the interface also occurs on roughly the same dimensionless times as in the experiment. To confirm the explanation proposed before, we plot the flow and polymer stress fields when the neck is at its thinnest (Fig. 3b). It is evident that the strong polymer tensile stress, due to the strain-hardening rheology, resists continued stretching and thinning of the neck, and suppresses partial coalescence.

3. Droplet self-assembly in nematic liquid crystals

When drops of an isotropic liquid are dispersed in a nematic liquid crystal (LC), surface anchoring—the tendency for LC molecules to orient in a certain direction relative to the interface—affects the near-field orientation and potentially disrupts the far-field orientation imposed on the bulk LC. This has two implications in our current context. First, the near- and far-field orientation may come into conflicts, with the result of producing orientational defects in the nematic (de Gennes & Prost, 1993; Larson, 1999). Second, the droplets can interact with each other through the distortional elasticity in the bulk, and self-assemble into patterns. In the process discussed below, the defects turn out to be the agent for self-assembly.

3.1. Experimental observations

Poulin and coworkers (Poulin *et al.*, 1997b) reported that water droplets suspended in a nematic liquid crystal (LC) organize themselves into a chain, with a more or less constant spacing between neighboring droplets. This was later confirmed by spectacular pictures of parallel chains that form by self-assembly of silicone oil droplets in a nematic medium (Loudet *et al.*, 2000) (Fig. 4a). More recently, 2D colloidal crystals have been made via self-assembly of colloidal particles in a nematic LC (Musevic *et al.*, 2006) (Fig. 4b).

In these observations, water and silicone-oil droplets possess *homeotropic* anchoring on the interface, perpendicular to the surface. When droplets line up into regular chains, each is always accompanied by a satellite point defect (Feng & Zhou, 2004). Poulin *et al.* (1997b) proposed an explanation for the self-assembly based on an analogy to electric dipoles. The droplet and its satellite point defect form a dipole, say pointing from the drop center to the defect. When two droplets are nearby, they interact through the equivalent of dipole-dipole attraction in electrostatics. The physical origin of the attraction is distortional elasticity in LC. When two such dipoles are lined up in the same direction, distortional energy is

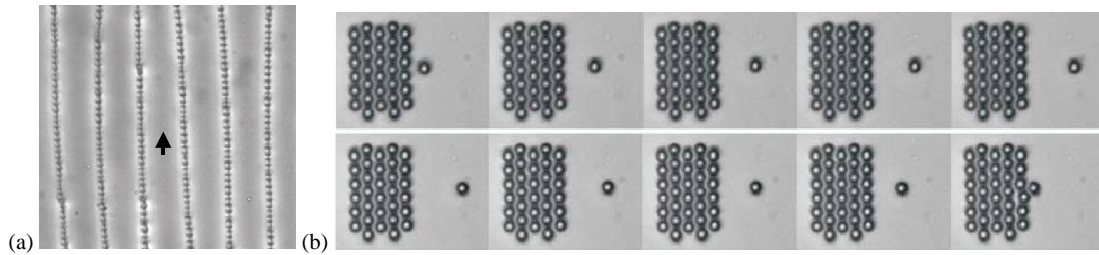


Fig. 4 (a) Silicone oil droplets, about $2\ \mu\text{m}$ in size, arrange themselves into roughly equally spaced lines along the direction of the nematic director (indicated by the black arrow). Adapted from Loudet *et al.* (2000) with permission, ©2000 Macmillan Magazines Ltd. (b) Chains of silica particles, $2.32\ \mu\text{m}$ in diameter, form a regular 2D crystal in a nematic LC. From left to right, the frames at advancing times show the interaction between the single particle and the chains. Adapted from Musevic *et al.* (2006) with permission, ©2006 by the American Association for the Advancement of Science.

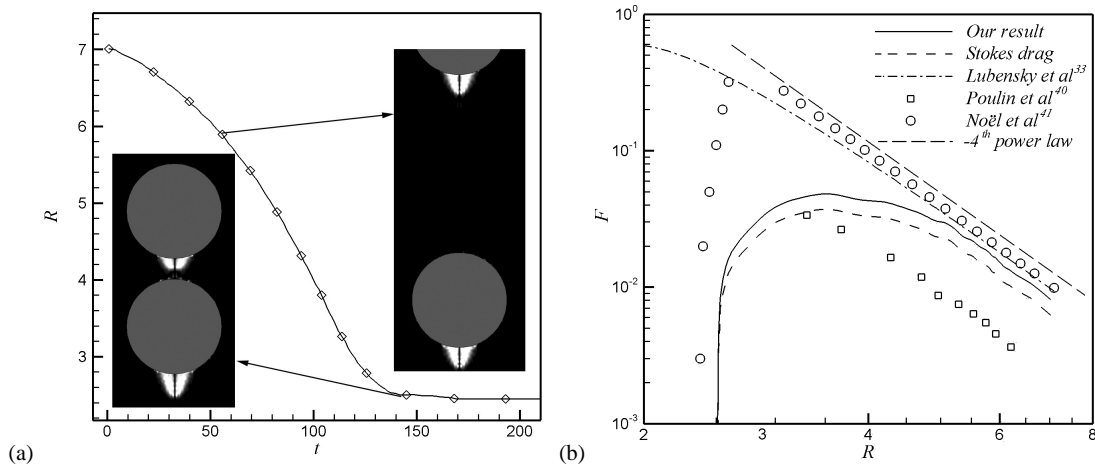


Fig. 5 Attraction between two droplets bearing satellite point defects placed in the parallel configuration. (a) The distance between the centers of the droplets decreasing as the two droplets attract each other. The two insets show the birefringence patterns around the defects computed from the director field. The point defect sits at the tip of the two bright lobes. (b) The attraction force as a function of the droplets' separation, compared with the dipole formula (Lubensky *et al.*, 1998) and experimental data (Noël *et al.*, 2006; Poulin *et al.*, 1997a). Note that both axes are in logarithmic scale and the long-range attraction exhibits a $F \sim R^{-4}$ power law. Adapted from Zhou *et al.* (2008) with permission, ©2008 by the American Chemical Society.

reduced when the two move toward each other until an optimal center-to-center separation of roughly $2.6a$, a being the drop radius (Poulin *et al.*, 1997b). Thus, droplets form a line with uniform spacing between neighbors along the direction of the background nematic director. The same analogy also explains the repulsion between two chains in parallel, with their dipoles pointing in the same direction. Thus, the parallel chains maintain a more or less equal distance from each other in Fig. 4a. Furthermore, two chains with their dipolar directions opposite to each other (anti-parallel) should attract each other, and this explains the formation of the regular 2D arrays in Fig. 4b consisting of chains of alternating dipole directions. But the dipole analogy only holds when neighboring drops are far apart, and fails as they approach each other. Toward a rigorous understanding of the physics underlying the self-assembly, we use numerical computations to probe the pairwise interaction between two droplets and the self-assembly of many droplets.

3.2. Numerical simulations

The drop interfaces are again represented as diffuse interfaces as in Sec. 2.2. But the LC bulk rheology requires a new constitutive theory. We use the Ericksen-Leslie theory for LC hydrodynamics, with a unit vector \mathbf{n} , called the director, representing the average molecular orientation field (de Gennes & Prost, 1993). Homeotropic anchoring is imposed on the drop surfaces. The numerical algorithm is essentially the same as used in Sec. 2.2, although locally refined grid is needed for accurate resolution of the sharp gradients \mathbf{n} near defects (Yue *et al.*, 2006b; Zhou *et al.*, 2007a, 2008, 2007b).

To study pairwise interaction, we place two droplets in the so-called parallel configuration in an axisymmetric computational domain, with their “dipoles” in the same direction and along their line of centers. Under the effect of distortional elasticity, the droplets start to move toward each other (Fig. 5a). From this motion, one can estimate the elastic driving

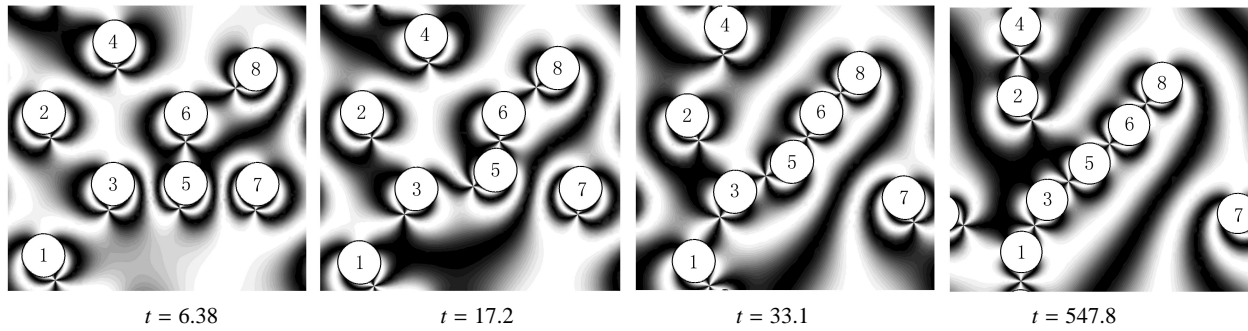


Fig. 6 Self-assembly of 8 drops in a doubly periodic domain. Time t is made dimensionless by $\eta a^2/K$. Adapted from Zhou *et al.* (2008) with permission, ©2008 by the American Chemical Society.

force on each droplet from the Stokes drag by neglecting inertia. This estimate turns out to be slightly below the true force computed from integrating the stress over the interface. Both forces are compared with prior theoretical and experimental results in Fig. 5b. The long-range attraction manifests a R^{-4} scaling, as is expected from the attraction between two electric dipoles (Lubensky *et al.*, 1998). As the separation decreases, however, the attraction force decreases sharply, falling below the dipole formula, and approaches zero toward $R = 2.45a$. The two experimental data sets indicate that the $F \propto R^{-4}$ power-law persists to smaller separations. But the equilibrium separation corresponding to $F = 0$ is in close agreement between computation and observations.

The dynamic simulation of droplet interaction thus confirms the idea that the long-range attraction between droplets in the parallel configuration resembles dipolar attraction. For smaller separations, the idea of dipole-dipole attraction no longer applies, and it certainly cannot account for the equilibrium separation and the repulsion between droplets that are too close to each other. This is where the dynamic computation provides results and insight that cannot come from the heuristic argument. Going beyond pairwise attraction, Zhou *et al.* (2008) have confirmed that a group of droplets in a 2D domain indeed form a chain along the undisturbed nematic director. To probe sideways interactions between chains of droplets, they arrange two chains with their “dipoles” either in the same direction (parallel) or reversed (anti-parallel) initially. Results show that the parallel chains repel each other, while the anti-parallel chains attract each other. These trends are in qualitative agreement with the experimental observations in Fig. 4b.

Finally, we place 8 identical droplets in random positions in a doubly periodic 2D domain, and observe their self-assembly (Fig. 6). The drop-drop interaction is dominated by longitudinal dipole-like attractions (when nearby droplets have their satellite defects on their line of centers) and sideways repulsions (when their dipoles are in the parallel configuration). For example, drops 3, 5 and 7 initially move away from each other sideways. Then drop 5 is attracted by drop 6, and is eventually pulled in between drops 3 and 6 to form a diagonal chain. Drops 1, 4 and 2 seem to form a vertical chain by themselves. Since the domain is doubly periodic, there is no prescribed background nematic orientation to which a chain may align. Thus, the two chains spontaneously assume different angles. Conceivably, they will eventually line up into a single long chain. Despite the small number of droplets in the simulation, the dynamic scenario of self-assembly exhibits the main features observed in reality (cf. Fig. 4a), and confirms that pairwise attraction (longitudinal) and repulsion (lateral) are the dominant mechanisms at play.

4. Interfacial behavior of ferrofluids

Ferrofluids are complex in the sense that additional magnetic force can be imposed on the fluid to drive exotic patterns. The magnetic stress tensor takes the form $\sigma_m = -\frac{1}{2}\mu_m H^2 \mathbf{I} + \mu_m \mathbf{H}\mathbf{H}$, where μ_m and \mathbf{H} are the magnetic permeability and the magnetic field, respectively, $H = |\mathbf{H}|$, and \mathbf{I} is the unit tensor. In the following, we discuss two scenarios where σ_m can be tuned to produce regular patterns of ferrofluid droplets.

4.1. Breakup and fingering in a steady magnetic field

The best known such pattern is the Rosensweig instability, which occurs in a layer of ferrofluid subject to a uniform vertical magnetic field. When the magnetic stress, perpendicular to the free surface, overcomes the surface tension, a regular pattern of pointed protrusions obtains (Cowley & Rosensweig, 1967; Richter & Barashenkov, 2005). This instability is governed by the magnetic Bond number $Bo_m = \mu_m H^2 / (\gamma \kappa_0)$, γ and κ_0 being surface tension and effective curvature, which indicates the ratio between magnetic and surface tension forces. If the ferrofluid layer is thin at the start,

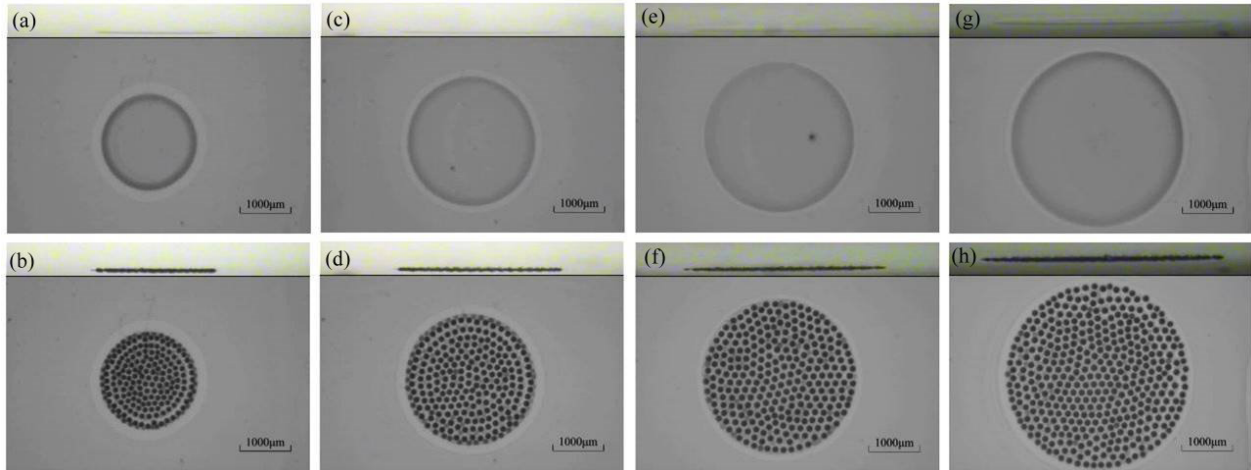


Fig. 7 Side and top views of ordered breakup of circular ferrofluid layers of various initial diameters under a vertical field $H = 765$ Oe. Top row: initial state; bottom row: final equilibrium state. From Chen & Li (2010) with permission, ©2010 American Institute of Physics.

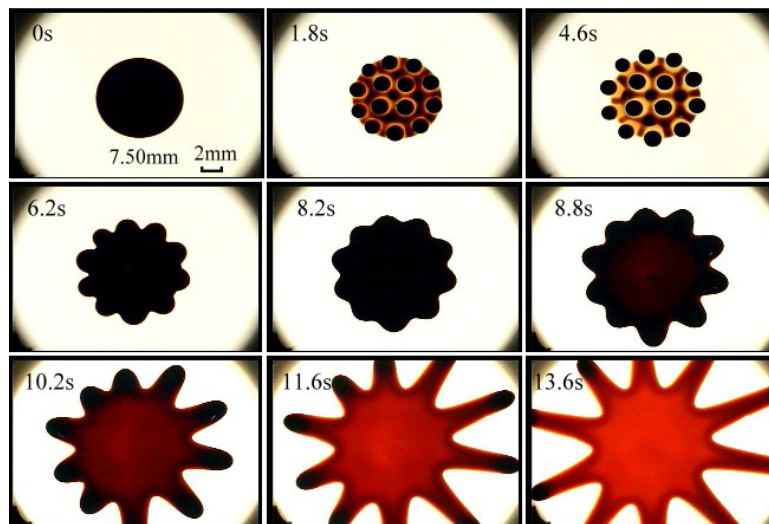


Fig. 8 Time evolution of a circular ferrofluid layer subjected first to a perpendicular magnetic field, and then to a purely radial field starting at $t = 6.2$ s. The initial drop diameter $D = 7.5$ mm, and $H_0 = 211$ Oe. From Chen *et al.* (2010) with permission, ©2010 American Society of Physics.

it is possible for the valleys between the Rosensweig peaks to dewet on the substrate, thereby breaking up the liquid film into micro-drops. Such a scenario was first reported by Chen & Cheng (2008). Given the non-uniform thickness of the initial liquid layer, larger drops typically appear in the middle. To produce micro-droplets of uniform size, Chen & Li (2010) achieved a flatter initial interface by tuning the wetting condition. Thus, orderly breakup of the ferrofluid film proceeds to produce numerous droplets of a uniform size (Fig. 7). The drop size d depends solely on the external field: $d \sim 1/H^2$. This scaling is as expected from the magnetic magnetic Bond number.

As the Rosensweig peaks or drops are magnetized by the vertical field, they may repel one another so their footprint expands radially on the substrate. To explore such radial expansion further, Chen *et al.* (2010) first used a vertical magnetic field to produce the drops as in Fig. 7, and then switched to a purely radial magnetic field of field strength $H = H_0 r/L$, H_0 being the characteristic field measured at $r = L$, the radius of the coil. This induces a radial body force $f_m \sim \mu_m r H_0^2$ that scales linearly with the radial coordinate r . The subsequent dynamics forms an interesting analogy to spin-coating, where a thin fluid layer is driven radially outward by centrifugal force (Spaid & Homsy, 1997). Similar to spin-coating, there exists a critical radius beyond which axisymmetric spreading gives way to a fingering instability. Fig. 8 illustrates this magnetically induced fingering process. Moreover, by varying the magnetic Bond number in the initial Rosensweig instability, one can control the number of droplets and subsequently the fingering pattern.

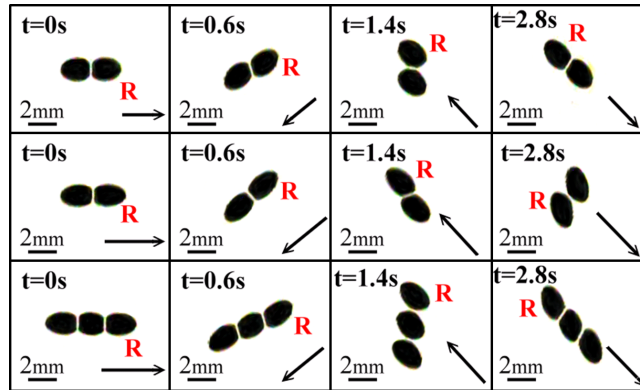


Fig. 9 Dynamics of doublets and triplets of drops in a magnetic field that is rotating counter-clockwise with a frequency of 1 revolution/s. (Top row) a doublet in a field $H_m = 47$ Oe; (middle row) a doublet with $H_m = 56.4$ Oe; (bottom row) a triplet with $H_m = 56.4$ Oe. The drop initially on the right is marked by letter R to show the orbital motion. The ferrofluid has a mineral oil base and the surrounding fluid is a glycerin-water mixture. From Chen *et al.* (2015) with permission, ©2015 Springer.

4.2. Drop dynamics in a rotating magnetic field

Now we turn to the dynamics of multiple ferrofluid drops in a spatially uniform magnetic field that is applied in the plane of the centers of the drops. While the droplet formation and fingering of the last subsection take place on a solid substrate, now we consider drops suspended in an immiscible liquid of matching density. As is well known, a single ferrofluid drop elongates in the field direction in a static uniform magnetic field (Afkhani *et al.*, 2010; Zhu *et al.*, 2011). In a rotating field, the drop elongates and also rotates or oscillates depending on the frequency (Lebedev *et al.*, 2003). Most of the earlier studies focused on a single ferrofluid drop. In recent experiments, Chen *et al.* (2015) explored the interaction among multiple drops in a rotating field, and discovered intriguing patterns such as “planetary motion” and self-assembly. We will summarize these newer findings in the following.

When two ferrofluid drops of equal size are placed in a static uniform field, both elongate in the field direction. They also attract each other and eventually align themselves into a doublet as shown in the top and middle row of Fig. 9 at $t = 0$. There is a thin film of the suspending fluid that prevents coalescence. The film drains at a rate that depends on the field strength, liquid viscosity and surface tension, and coalescence may or may not occur within the duration of observation. This alignment behavior can be understood by thinking of each drop as a magnetic dipole. At a separation of r , the dipole-dipole attraction has a radial and an azimuthal component (Banerjee *et al.*, 2012; Melle *et al.*, 2003):

$$F_r \sim \frac{(1 - 3 \cos^2 \Delta\theta_L)}{r^4}, \quad F_\theta \sim \frac{\sin(2\Delta\theta_L)}{r^4}, \quad (2)$$

where $\Delta\theta_L$ is the instantaneous angle from the line of centers to the external field direction. These forces eventually result in an equilibrium alignment of particles along the external field, with $\Delta\theta_L = 0$ and $F_\theta = 0$. Of course, this point-dipole model cannot predict the deformation of drops. Similarly, three drops form a triplet (bottom row of Fig. 9).

If the field rotates, doublets and triplets of drops exhibit interesting behavior (Fig. 9). First, each drop undergoes synchronized spin with the external field as commonly observed in the cases of single drop (Lebedev *et al.*, 2003). Meanwhile, the interaction between the drops results in an orbital rotation around the centroid of the array. Averaged over time, this “planetary revolution” is in the same sense as the external magnetic field, but at a much lower rate. Besides, the speed of the orbital motion is not constant, but tends to fluctuate periodically as the hydrodynamic resistance on the drops changes with the relative position and orientation of the drops. Figure 10 plots the orientation of the line of centers at different times. The orbital motion consists of counterclockwise rotation interspersed with short episodes of reversal. The average rate of orbital motion is higher for shorter chains and stronger fields. The above observations can be understood from the azimuthal force in the point-dipole model. As the field rotates continuously, the line of centers always lags the field in phase ($\Delta\theta_L > 0$). The azimuthal force thus induced (see Eq. 2) drives the drops to revolve around each other in an orbital motion. The intermittent reverse rotation occurs at times when the phase lag exceeds 90° , which temporarily changes the sign of the azimuthal force prescribed by the point-dipole mode. This fluctuating orbital motion is similar to the “trajectory shift” observed for magnetic particle chains in an oscillating field (Li *et al.*, 2013a,b).

Longer chains with a greater number of drops tend to break up in the rotating field. The magnetic field promotes the integrity of the chain by the dipolar attraction. However, its orbital rotation incurs hydrodynamic drag that is higher

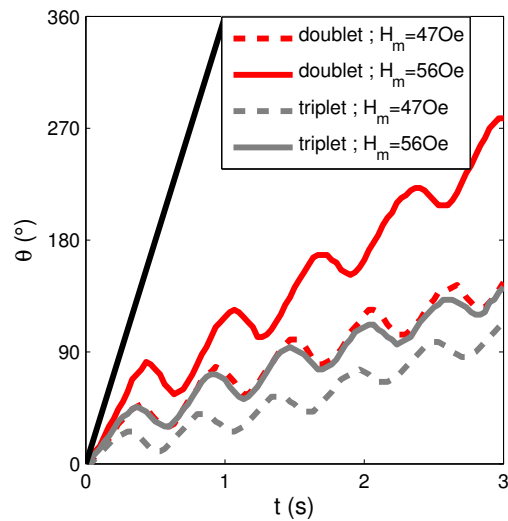


Fig. 10 Planetary revolution of drop arrays. For comparison, rotation of the external field (at $360^\circ/\text{s}$) is indicated by the black solid line. Forward (counterclockwise) rotation is interspersed with brief intervals of backward rotation. From Chen *et al.* (2015) with permission, ©2015 Springer.

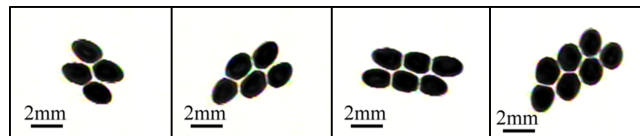


Fig. 11 The most stable patterns of rotating arrays with various numbers of ferrofluid drops. Longer chains cannot be sustained because of significant variations of the hydrodynamic drags among the drops. From Chen *et al.* (2015) with permission, ©2015 Springer.

on the drops nearer the end of the chain, which revolve at higher speed. Thus, a long chain often breaks up into shorter chains. Figure 11 illustrates stable configurations that develop following such breakup for up to seven droplets. Remarkably, the drops arrange themselves into regular patterns. Each drop still spins in synchrony with the external field, and the regular array as a whole rotates slowly as well, with forward (counterclockwise) rotation punctuated by brief periods of reverse rotation, similar to Fig. 10. A movie showing the rotation of a six-drop array can be viewed online: <https://www.youtube.com/watch?v=8nFUTeZxSBU>

5. Concluding remarks

In this brief review, we have demonstrated the variety of novel interfacial dynamics for complex fluids. The microstructure of these fluids affords us the opportunity to manipulate the bulk and interfacial flows, thereby producing rich patterns unseen in simple fluids. The key insight from these observations is that the coupling among different length scales, from the microstructural to the interfacial and in turn to the macroscopic, can dictate the outcome of the flow.

For the first two problems reviewed, suppression of partial coalescence by viscoelasticity and self-assembly of drops driven by distortional elasticity in the suspending liquid crystal, we have presented fluid-dynamic computations that provide a detailed and quantitative analysis of the phenomena. For the drop dynamics in ferrofluids, on the other hand, we contented ourselves with rough analogies to dipolar interactions. Although capable of rationalizing the most salient features of the flow, the dipole analogy is at best a qualitative guideline. For one, it fails at short distances, and the ferrofluid drops do approach each other to such a degree that their separation becomes much smaller than the drop size. The dipole analogy, strictly speaking, cannot be used for such situations.

A review of the literature shows that little quantitative analysis has been done on ferrofluid drop dynamics. Single-drop deformation has been studied before (Afkhani *et al.*, 2010; Zhu *et al.*, 2011), but much remains to be explored for drop-drop interaction and pattern formation. Open questions include the hydrodynamic mechanisms for drop-drop alignment, the planetary motion of drops in arrays and clusters, and self-assembly of a larger number of drops in rotating fields. Also notable is the non-coalescence among drops during planetary revolution, despite the magnetically induced attraction between the drops (see Eq. 2) and their close proximity (see Fig. 11). In principle, one has to overcome two

difficulties in carrying out full-field flow simulations of these phenomena. First, one needs a highly accurate and efficient computational scheme to handle the interfacial deformation and motion. The phase-field method described here is one of several options. Second, one also needs to solve for the induced magnetic field together with the flow field, such that the two-phase Navier-Stokes equations can be solved with the magnetic stress σ_m taken into account. Such simulations will contribute to a thorough understanding of interfacial dynamics in ferrofluid.

As mentioned before, we have not strived to be comprehensive in this review. Instead, we have selected a few representative examples to illustrate the anomalous interfacial dynamics of complex fluids. Our hope is that this may stimulate new research in this area, which covers a very wide range of materials of scientific and practical interest.

Acknowledgements: We acknowledge support by the NSERC (Grant 05862) and the MOST (104-2221-E-009-142-MY3). The collaboration between the authors was also supported by the Peter Wall Institute for Advanced Studies at UBC, which funded JJF as a Wall Scholar and CYC as an International Visiting Research Scholar during the 2014-2015 academic year.

References

- AFKHAM, S., TYLER, A. J., RENARDY, Y., RENARDY, M., ST. PIERRE, T. G., WOODWARD, R. C. & RIFFLE, J. S. 2010 Deformation of a hydrophobic ferrofluid droplet suspended in a viscous medium under uniform magnetic fields. *J. Fluid Mech.* **663**, 358–384.
- BANERJEE, U., BIT, P., GANGULY, R. & HARDT, S. 2012 Aggregation dynamics of particles in a microchannel due to an applied magnetic field. *Microfluid. Nanofluid.* **13**, 565–577.
- BIRD, R. B., ARMSTRONG, R. C. & HASSAGER, O. 1987a *Dynamics of Polymeric Liquids, Vol. 1. Fluid Mechanics*. New York: Wiley.
- BIRD, R. B., CURTISS, C. F., ARMSTRONG, R. C. & HASSAGER, O. 1987b *Dynamics of Polymeric Liquids, Vol. 2. Kinetic Theory*. New York: Wiley.
- BLANCHETTE, FRANCOIS & BIGIONI, TERRY P. 2006 Partial coalescence of drops at liquid interfaces. *Nature Phys.* **2**, 254–257.
- BLOISI, FRANCESCO & VICARI, LUCIANO ROSARIO MARIA 2012 Polymer dispersed lcls. In *Handbook of Visual Display Technology* (ed. Janglin Chen, Wayne Cranton & Mark Fihn), pp. 1565–1585. Springer.
- CHARLES, G. E. & MASON, S. G. 1960 The mechanism of partial coalescence of liquid drops at liquid/liquid interfaces. *J. Colloid Sci.* **15**, 105–122.
- CHEN, C.-Y. & CHENG, Z.-Y. 2008 An experimental study on Rosensweig instability of a ferrofluid droplet. *Phys. Fluids* **20**, 054105.
- CHEN, C.-Y., HSUEH, H.-C., WANG, S.-Y. & LI, Y.-H. 2015 Self-assembly and novel planetary motion of ferrofluid drops in a rotational magnetic field. *Microfluid Nanofluid* **18**, 795–806.
- CHEN, C.-Y. & LI, C.-S. 2010 Ordered microdroplet formations of thin ferrofluid layer breakups. *Phys. Fluids* **22**, 014105.
- CHEN, C.-Y., WU, W.-L. & MIRANDA, J. A. 2010 Magnetically induced spreading and pattern selection in thin ferrofluid drops. *Phys. Rev. E* **82**, 056321.
- CHEN, X., MANDRE, S. & FENG, J.J. 2006a Partial coalescence between a drop and a liquid-liquid interface. *Phys. Fluids* **18**, 051705.
- CHEN, X., MANDRE, S. & FENG, J. J. 2006b An experimental study of the coalescence between a drop and an interface in newtonian and polymeric liquids. *Phys. Fluids* **18**, 092103.
- COWLEY, M. D. & ROSENSWEIG, R. E. 1967 The interfacial stability of a ferromagnetic fluid. *J. Fluid Mech.* **30**, 671–688.
- DOI, M. & EDWARDS, S. F. 1986 *The Theory of Polymer Dynamics*. New York: Oxford.

- FENG, J. J., LIU, C., SHEN, J. & YUE, P. 2005 An energetic variational formulation with phase field methods for interfacial dynamics of complex fluids: advantages and challenges. In *Modeling of Soft Matter* (ed. M.-C. T. Calderer & E. M. Terentjev), pp. 1–26. New York: Springer.
- FENG, J. J. & ZHOU, C. 2004 Orientational defects near colloidal particles in a nematic liquid crystal. *J. Colloid Interface Sci.* **269**, 72–78.
- FONTELOS, M. A. & LI, J. 2004 On the evolution and rupture of filaments in Giesekus and FENE models. *J. Non-Newtonian Fluid Mech.* **118**, 1–16.
- DE GENNES, P. G. & PROST, J. 1993 *The Physics of Liquid Crystals*. New York: Oxford.
- GILET, T., MULLENNERS, K., LECOMTE, J. P., VANDEWALLE, N. & DORBOLO, S. 2007 Critical parameters for the partial coalescence of a droplet. *Phys. Rev. E* **75**, 036303.
- HONEY, E. M. & KAVEHPUR, H. P. 2006 Astonishing life of a coalescing drop on a free surface. *Phys. Rev. E* **73**, 027301.
- LARSON, R. G. 1999 *The Structure and Rheology of Complex Fluids*. New York: Oxford.
- LEBEDEV, ALEXANDER V, ENGEL, ANDREAS, MOROZOV, KONSTANTIN I & BAUKE, HEIKO 2003 Ferrofluid drops in rotating magnetic fields. *New J. Phys.* **5**, 57.
- LI, Y.-H., LIN, H.-C. & CHEN, C.-Y. 2013a Steering of magnetic micro-swimmers. *IEEE Trans. Magn.* **49**, 4120–4123.
- LI, Y.-H., LIN, H.-C. & CHEN, C.-Y. 2013b Trajectory shift of magnetic microchains in an oscillating field. *Microfluid Nanofluid* **14**, 832–838.
- LOUDET, J. C., BAROIS, P. & POULIN, P. 2000 Colloidal ordering from phase separation in a liquid crystalline continuous phase. *Nature* **407**, 611–613.
- LUBENSKY, T. C., PETTEY, DAVID, CURRIER, NATHAN & STARK, HOLGER 1998 Topological defects and interactions in nematic emulsions. *Phys. Rev. E* **57**, 610–625.
- MELLE, S., CALDERON, O. G., RUBIO, M. A. & FULLER, G. G. 2003 Microstructure evolution in magnetorheological suspensions governed by Mason number. *Phys. Rev. E* **68**, 041503.
- MOHAMED-KASSIM, Z. & LONGMIRE, E. K. 2004 Drop coalescence through a liquid/liquid interface. *Phys. Fluids* **16**, 2170–2181.
- MUSEVIC, IGOR, SKARABOT, MIHA, TKALEC, UROS, RAVNIK, MIHA & ZUMER, SLOBODAN 2006 Two-Dimensional Nematic Colloidal Crystals Self-Assembled by Topological Defects. *Science* **313**, 954–958.
- NIKOLOV, A. D. & WASAN, D. T. 1995 Effects of surfactant on multiple stepwise coalescence of single drops at liquid-liquid interfaces. *Ind. Eng. Chem. Res.* **34**, 3653–3661.
- NOËL, C. M., BOSSIS, G., CHAZE, A.-M., GIULIERI, F. & LACIS, S. 2006 Measurement of elastic forces between iron colloidal particles in a nematic liquid crystal. *Phys. Rev. Lett.* **96**, 217801.
- ODENBACH, S., ed. 2002 *Ferrofluids: Magnetically Controllable Fluids and Their Applications*. New York: Springer.
- OLIVEIRA, M. S. N. & MCKINLEY, G. H. 2005 Iterated stretching and multiple beads-on-a-string phenomena in dilute solutions of highly extensible flexible polymers. *Phys. Fluids* **17**, 071704.
- POULIN, P., CABUIL, V. & WEITZ, D. A. 1997a Direct measurement of colloidal forces in an anisotropic solvent. *Phys. Rev. Lett.* **79**, 4862–4865.
- POULIN, P., STARK, H., LUBENSKY, T. C. & WEITZ, D. A. 1997b Novel colloidal interactions in anisotropic fluids. *Science* **275**, 1770–1773.
- RICHTER, R. & BARASHENKOV, I. V. 2005 Two-dimensional solitons on the surface of magnetic fluids. *Phys. Rev. Lett.* **94**, 184503.

- ROSENSWEIG, R. E. 1997 *Ferrohydrodynamics*. Mineola, New York: Dover.
- SPAID, M. A. & HOMSY, G. M. 1997 Stability of viscoelastic dynamic contact lines: An experimental study. *Phys. Fluids* **9**, 823–832.
- THOMAS, S., GROHENS, Y. & JYOTISHKUMAR, P., ed. 2015 *Characterization of Polymer Blends: Miscibility, Morphology, and Interfaces*. New York: Wiley.
- THORODDSEN, S. T. & TAKEHARA, K. 2000 The coalescence cascade of a drop. *Phys. Fluids* **12** (6), 1265–1267.
- YUE, P., FENG, J. J., LIU, C. & SHEN, J. 2004 A diffuse-interface method for simulating two-phase flows of complex fluids. *J. Fluid Mech.* **515**, 293–317.
- YUE, P., ZHOU, C. & FENG, J. J. 2006a A computational study of the coalescence between a drop and an interface in Newtonian and viscoelastic fluids. *Phys. Fluids* **18**, 102102.
- YUE, P., ZHOU, C., FENG, J. J., OLLIVIER-GOOCH, C. F. & HU, H. H. 2006b Phase-field simulations of interfacial dynamics in viscoelastic fluids using finite elements with adaptive meshing. *J. Comput. Phys.* **219**, 47–67.
- ZHOU, C., YUE, P. & FENG, J. J. 2007a The rise of Newtonian drops in a nematic liquid crystal. *J. Fluid Mech.* **593**, 385–404.
- ZHOU, C., YUE, P. & FENG, J. J. 2008 Dynamic simulation of droplet interaction and self-assembly in a nematic liquid crystal. *Langmuir* **24**, 3099–3110.
- ZHOU, C., YUE, P., FENG, J. J., LIU, C. & SHEN, J. 2007b Heart-shaped bubbles rising in anisotropic liquids. *Phys. Fluids* **19**, 041703.
- ZHOU, C., YUE, P., FENG, J. J., OLLIVIER-GOOCH, C. F. & HU, H. H. 2010 3D phase-field simulations of interfacial dynamics in Newtonian and viscoelastic fluids. *J. Comput. Phys.* **229**, 498–511.
- ZHU, G. P., NGUYEN, N. T., RAMANUJAN, R. & HUANG, X. Y. 2011 Nonlinear deformation of a ferrofluid droplet in a uniform magnetic field. *Langmuir* **27**, 14834–14841.